A Finite-Element Contrast Source Inversion Method for Microwave Tomography

Amer Zakaria, Colin Gilmore, and Joe LoVetri

Department of Electrical and Computer Engineering
University of Manitoba, Winnipeg, MB, R3T 5V6, Canada
azakaria@ee.umanitoba.ca, cgilmore@ee.umanitoba.ca, Joe_LoVetri@umanitoba.ca

Abstract: A new inversion algorithm based on the contrast source inversion (CSI) and a finite-element method (FEM) discretization of the scattered-field differential operator is presented. The unknown electric properties are represented as nodal values on a two-dimensional (2D) arbitrary triangular mesh using linear basis functions. The use of FEM to represent the operator allows the flexibility of having an inhomogeneous background medium, as well as the ability to accurately model any boundary shape or type: both conducting and absorbing. The resulting sparse and symmetric FEM matrix equation can be solved efficiently, and it is shown how its solution can be used to calculate the gradient operators required in the conjugate-gradient CSI update without storing the inverse of the FEM matrix. The inversion algorithm is applied to conductive-enclosure and unbounded-region microwave tomography configurations where the 2D transverse magnetic (TM) approximation can be applied. Examples using synthetic scattered-field data are provided.

Keywords: Finite-Element Method, Contrast Source Inversion, Microwave Tomography.

1. Introduction

The contrast source inversion (CSI) technique is a state-of-the-art algorithm that has had much success with solving the nonlinear ill-posed electromagnetic inverse scattering problem associated with microwave tomography (MWT) [1]. Recently a finite-difference contrast source inversion method (FD-CSI) has been introduced that provides several advantages, especially for biomedical applications where prior information can be more easily included than in integral equation based formulations of CSI [2]. The Finite-Element Method (FEM) CSI algorithm introduced here retains all the advantages of FD-CSI and overcomes two major problems inherent in FD-CSI. First, FD discretizations make it difficult to accurately model arbitrarily shaped boundaries, whether of the enclosure or of the unknown object, because of the use structured rectangular grids requiring stair-stepping of curved boundaries. Although this is not an issue for unbounded-region configurations, where absorbing boundary conditions have successfully been used to truncate the FD grid [3], it does become an issue for MWT configurations with conductive enclosures of arbitrary shape [4]. It also becomes problematic when including prior information about the target which may be of arbitrary shape. In addition, using arbitrary triangular meshes allows the possibility of increasing the resolution of the reconstruction where it is needed in an adaptive way. That is, a higher density mesh can be imposed, either adaptively or initially if prior information is available, in regions where the spatial distribution of the electrical parameters is varying highly.

In this paper, a novel inversion algorithm based on the finite-element method combined with the contrast source inversion is presented. This algorithm is applied to two-dimensional (2D) transverse magnetic (TM) problems. In each problem, the domain is divided into triangular elements, and the electric properties of the unknown object are reconstructed at the nodes of triangles within an imaging domain. The boundary of the problem can have any arbitrary shape and can be of any type. Within the framework of the CSI method two variables (the contrast source and contrast) are updated sequentially. The contrast source variables are updated by a conjugate-gradient method with Polak-Ribière directions to minimize the CSI cost functional, assuming the contrast variables to be constant. Then, because the functional becomes quadratic in the contrast variables, they can be updated analytically.

2. Problem Formulation

For the 2D TM problem we assume z-polarized electric fields and an $\exp(j\omega t)$ time dependency. The unknown inhomogeneous object of interest (OI), assumed to be isotropic, is located in a bounded imaging domain $\mathcal{D}$ within a background region of known electric properties. The permeability of the OI and background is taken to be that of free-space μ_0. The surrounding medium is enclosed within a boundary denoted by Γ that contains the MWT setup and can be of any shape, size, or type. The complex relative permittivity of the OI is denoted by $\epsilon_r(\boldsymbol{r})$, where $\boldsymbol{r} = (x, y)$ is the 2D position vector. The corresponding contrast is defined as $\chi(\boldsymbol{r}) = \big(\epsilon_r(\boldsymbol{r}) - \epsilon_b\big)/\epsilon_b$, where ϵ_b is the relative complex permittivity of the background (outside $\mathcal{D}$, $\chi(\boldsymbol{r}) = 0$).

It is assumed that the incident field in the imaging domain $\mathcal{D}$ produced by one of the T transmitters is known. In our case the transmitters are 2D point sources and all scattered-field data is collected at points located on a measurement domain $\mathcal{S}$. For a source t, the scattered electric field E_t^{sct} is governed by the scalar Helmholtz equation given by

$$\nabla^2 E_t^{\text{sct}}(\boldsymbol{r}) + k_b^2 E_t^{\text{sct}}(\boldsymbol{r}) = -k_b^2 w_t(\boldsymbol{r}), \tag{1}$$

where $k_b = \omega\sqrt{\mu_0\epsilon_0\epsilon_b}$ is the background wavenumber and $w_t(\boldsymbol{r}) \triangleq \chi(\boldsymbol{r})E_t(\boldsymbol{r})$, with E_t the total field.

Solving for the scattered field E_t^{sct} requires that boundary conditions (BCs) on Γ be defined. For a conductive-enclosure system perfect electrical conductor (PEC) boundary conditions are used resulting in the homogeneous Dirichlet BC. Unbounded-region systems require that Sommerfeld radiating boundary conditions be imposed.

3. Discretization Using the Finite Element Method

The problem domain (Ω) is discretized into a mesh of first-order triangular elements defined by N nodes. At each node, a linear basis function is specified, the parameters of which depend solely on the geometry of the mesh. We use the standard Rayleigh-Ritz formulation of FEM [5] to solve (1) which, irrespective of the type of BCs used, produces an FEM matrix equation of the form

$$\left[\mathbf{S} - k_b^2\mathbf{T}\right] E_t^{\text{sct}} = k_b^2\mathbf{T}w_t. \tag{2}$$

Here $\mathbf{S}$ is the stiffness matrix, which depends on the BCs, and $\mathbf{T}$ is the mass matrix. The vectors $E_t^{\text{sct}} \in \mathbb{C}^N$ and $w_t \in \mathbb{C}^N$ contain the nodal values of the scattered field and contrast source for transmitter t.

Entries in the ith row and jth column of the stiffness matrix (not arising from the boundary-integral term) and the mass matrix are given by

$$S_{i,j} = \int_\Omega \nabla\lambda_i \cdot \nabla\lambda_j \, d\Omega \quad \text{and} \quad T_{i,j} = \int_\Omega \lambda_i\lambda_j \, d\Omega, \tag{3}$$

where λ_i and λ_j are the linear basis functions defined at the ith and jth nodes respectively, and ∇ is a spatial gradient operator.

The Sommerfeld radiation BCs are modeled using the following second-order radiating BCs [5]:

$$\frac{\partial E_t^{\text{sct}}(\boldsymbol{r})}{\partial n} + \gamma_1(\boldsymbol{r}) E_t^{\text{sct}}(\boldsymbol{r}) = -\gamma_2(\boldsymbol{r}) \frac{\partial^2 E_t^{\text{sct}}(\boldsymbol{r})}{\partial s^2} \quad \text{for} \quad \boldsymbol{r} \in \Gamma, \tag{4}$$

where $\hat{n}$ denotes the outward-normal unit vector, s is the arc length measured along the boundary,

$$\gamma_1(\boldsymbol{r}) = jk_b(\boldsymbol{r}) + \frac{\kappa(s)}{2} - \frac{\kappa^2(s)}{8(j\kappa(s) - k_b(\boldsymbol{r}))} \quad , \quad \gamma_2(\boldsymbol{r}) = -\frac{j}{2(j\kappa(s) - k_b(\boldsymbol{r}))}, \tag{5}$$

and $\kappa(s)$ is the curvature of the boundary at s. The FEM formulation produces a boundary integral term which contributes to the (i,j)th element of $\mathbf{S}$ as

$$S_{i,j}^{\Gamma} = \int_{\Gamma} \left(\gamma_1 \lambda_i^{\Gamma} \lambda_j^{\Gamma} - \gamma_2 \frac{\partial \lambda_i^{\Gamma}}{\partial s} \frac{\partial \lambda_j^{\Gamma}}{\partial s} \right) d\Gamma, \tag{6}$$

where λ_i^{Γ} and λ_j^{Γ} are linear boundary basis functions defined for nodes i and j on Γ.

The solution E_t^{sct} can be computed efficiently because matrices $\mathbf{S}$ and $\mathbf{T}$ are sparse and symmetric. In addition, these matrices are independent of the transmitter location as well as the nature of the OI, so they are assembled only once, saved, and recalled when necessary.

4. The Inversion Algorithm

To describe the CSI algorithm more effectively, it is advantageous to introduce some notation for several matrix operators. The FEM matrix operator $\boldsymbol{\mathcal{L}} \in \mathbb{C}^{N \times N}$ is defined as

$$E_t^{\text{sct}} = \boldsymbol{\mathcal{L}}[w_t] = \left(\mathbf{S} - k_b^2 \mathbf{T} \right)^{-1} k_b^2 \mathbf{T}[w_t]. \tag{7}$$

Next, to obtain field values at measurement points on the surface $\mathcal{S}$ or at the nodes within domain $\mathcal{D}$ two matrix operators are defined. The $\boldsymbol{\mathcal{M}}_{\mathcal{S}}$ operator returns the field values at measurement points on $\mathcal{S}$; these points can be inside or outside the FEM mesh (outside, for unbounded problems). If the points are within the mesh, $\boldsymbol{\mathcal{M}}_{\mathcal{S}}$ will interpolate using the FEM basis functions, while if the points are outside the mesh, Huygens' principle is used [5]. The $\boldsymbol{\mathcal{M}}_{\mathcal{D}}$ operator selects the fields at all nodes within the imaging domain $\mathcal{D}$. Both matrices operate on vectors containing field values at mesh nodes.

Using this notation, the CSI cost functional to be minimized, which is a function of the contrast sources w and contrasts χ, is written as

$$\mathcal{F}(\chi, w) = \frac{\sum_t \| f_t - \boldsymbol{\mathcal{M}}_{\mathcal{S}} \boldsymbol{\mathcal{L}}[w_t] \|_{\mathcal{S}}^2}{\sum_t \| f_t \|_{\mathcal{S}}^2} + \frac{\sum_t \left\| \chi \odot E_{t,\mathcal{D}}^{\text{inc}} - w_{t,\mathcal{D}} + \chi \odot \boldsymbol{\mathcal{M}}_{\mathcal{D}} \boldsymbol{\mathcal{L}}[w_t] \right\|_{\mathcal{D}}^2}{\sum_t \left\| \chi \odot E_{t,\mathcal{D}}^{\text{inc}} \right\|_{\mathcal{D}}^2}, \tag{8}$$

where $f_t \in \mathbb{C}^R$ is the measured data at the R receiver locations and $\chi \in \mathbb{C}^I$ contains the contrast nodal-values at the I nodes inside the imaging domain. Here, $\boldsymbol{\mathcal{M}}_{\mathcal{S}} \in \mathbb{C}^{R \times N}$ and $\boldsymbol{\mathcal{M}}_{\mathcal{D}} \in \mathbb{R}^{I \times N}$ are matrix operators, $E_{t,\mathcal{D}}^{\text{inc}} = \boldsymbol{\mathcal{M}}_{\mathcal{D}}[E_t^{\text{inc}}]$ is used to denote the incident field inside the imaging domain, and the notation $a \odot b$ denotes the Hadamard (element-wise) product. The first term in the cost functional is known as the data misfit $\mathcal{F}^{\mathcal{S}}(w)$ and the second term is called the domain equation error $\mathcal{F}^{\mathcal{D}}(\chi, w)$.

On the FEM mesh the L_2-norms in the cost functional are calculated as

$$\|x\|_{\mathcal{S}}^2 = \langle x, x\rangle_{\mathcal{S}} = x^H x, \quad \text{and} \quad \|x\|_{\mathcal{D}}^2 = \langle x, x\rangle_{\mathcal{D}} = x^H \mathbf{T}_{\mathcal{D}} x, \tag{9}$$

where x is an arbitrary vector, superscript H denotes the Hermitian (complex conjugate transpose), and $\mathbf{T}_{\mathcal{D}}$ is the mass matrix restricted to the nodes within the imaging domain $\mathcal{D}$. The (i,j)th element of $\mathbf{T}_{\mathcal{D}}$ is calculated as in (3) except with the integration taken only over $\mathcal{D}$.

The CSI method updates the unknown contrast sources w_t and contrast χ in two sequential steps. In the first step, the w_t are updated by a conjugate-gradient (CG) method with Polak-Ribière search directions, and in the second step, χ is calculated analytically such that the error in the domain equation is minimized. The first update equation for the CSI method is

$$w_{t,n} = w_{t,n-1} + \alpha_{t,n} d_{t,n}, \tag{10}$$

where subscript n is the iteration number and $\alpha_{t,n}$ is the update step-size. The Polak-Ribière search directions $d_{t,n}$ are calculated by the following formula:

$$d_{t,n} = g_{t,n} + \frac{\sum_k \langle g_{k,n}, g_{k,n} - g_{k,n-1}\rangle_{\mathcal{D}}}{\sum_k \|g_{k,n-1}\|_{\mathcal{D}}^2} d_{t,n-1}, \tag{11}$$

where $g_{t,n}$ is the gradient of the cost function $\mathcal{F}(\chi, w)$ with respect to the contrast sources w_t.

It can be shown, using a procedure similar to [3], that the gradient $g_{t,n}$ is

$$g_{t,n} = -\eta^{\mathcal{S}} \mathbf{T}_{\mathcal{D}}^{-1} \widetilde{\mathbf{T}}^H \boldsymbol{\mathcal{L}}_b^H [\boldsymbol{\mathcal{M}}_{\mathcal{S}}^H \rho_{t,n-1}] - \eta_n^{\mathcal{D}} \mathbf{T}_{\mathcal{D}}^{-1} \Big(\mathbf{T}_{\mathcal{D}} r_{t,n-1} - \widetilde{\mathbf{T}}^H \boldsymbol{\mathcal{L}}_b^H [\boldsymbol{\mathcal{M}}_{\mathcal{D}}^H \overline{X}_{n-1} \odot \mathbf{T}_{\mathcal{D}} r_{t,n-1}] \Big), \tag{12}$$

where the overbar donates the complex conjugate, $\widetilde{\mathbf{T}} \in \mathbb{R}^{N \times I}$ is a matrix that contains the columns of $\mathbf{T}$ corresponding to the nodes in $\mathcal{D}$, $\boldsymbol{\mathcal{L}}_b \triangleq k_b^2 \big(\mathbf{S} - k_b^2 \mathbf{T}\big)^{-1}$ is a matrix operator, the normalization factors $\eta^{\mathcal{S}}$ and $\eta_n^{\mathcal{D}}$ are

$$\eta^{\mathcal{S}} = \left(\sum_t \|f_t\|_{\mathcal{S}}^2 \right)^{-1} \quad \text{and} \quad \eta_n^{\mathcal{D}} = \left(\sum_t \left\| \chi_{n-1} \odot E_{t,\mathcal{D}}^{\text{inc}} \right\|_{\mathcal{D}}^2 \right)^{-1}, \tag{13}$$

and the error terms $\rho_{t,n-1}$ and $r_{t,n-1}$ are

$$\rho_{t,n-1} = f_t - \boldsymbol{\mathcal{M}}_{\mathcal{S}} \boldsymbol{\mathcal{L}} [w_{t,n-1}] \quad \text{and} \quad r_{t,n-1} = \chi_{n-1} \odot E_{t,\mathcal{D}}^{\text{inc}} - w_{t,\mathcal{D},n-1} + \chi_{n-1} \odot \boldsymbol{\mathcal{M}}_{\mathcal{D}} \boldsymbol{\mathcal{L}} [w_{t,n-1}]. \tag{14}$$

Note that $\widetilde{\mathbf{T}}$ and $\mathbf{T}_{\mathcal{D}}$ in the gradient arise because of the non-uniform mesh used in the FEM formulation of the inverse problem. For efficiency, the LU-decomposition is employed for $\mathbf{T}_{\mathcal{D}}^{-1}$ and the inverse matrices in $\boldsymbol{\mathcal{L}}$ and $\boldsymbol{\mathcal{L}}_b$.

After updating the contrast sources, the contrasts χ are evaluated by minimizing the domain equation $\mathcal{F}^{\mathcal{D}}(\chi, w)$. This results in the following sparse matrix equation for χ_n:

$$\left(\sum_t \mathbf{E}_{t,n} \mathbf{T}_{\mathcal{D}} \mathbf{E}_{t,n} \right) \chi_n = \sum_t \mathbf{E}_{t,n} \mathbf{T}_{\mathcal{D}} w_{t,n}. \tag{15}$$

Here $\mathbf{E}_{t,n} \in \mathbb{C}^{I \times I}$ is a diagonal matrix whose diagonal entities are the elements of vector $E_{t,n,\mathcal{D}} = E_{t,\mathcal{D}}^{\text{inc}} + \boldsymbol{\mathcal{M}}_{\mathcal{D}} \boldsymbol{\mathcal{L}} [w_{t,n}]$. The FEM-CSI algorithm is terminated when: (i) the number of iterations exceed a prescribed maximum, or (ii) the data misfit $\mathcal{F}^{\mathcal{S}}(w)$ is less than a prescribed value.

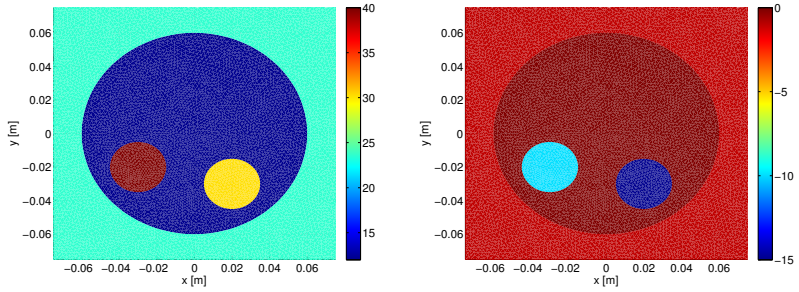

(a) Exact $Re(\epsilon_r)$ (b) Exact $Im(\epsilon_r)$

Fig. 1. Exact relative permittivity of OI.

5. Inversion Results

The FEM-CSI algorithm was successfully tested on several test cases using synthetic data created with our FEM solver but using meshes different from the ones used for the inversions. Here we show two sets of results for an OI which consists of three circular regions immersed in a lossy background medium of relative permittivity $\epsilon_r = 23.4 - j1.13$ at frequency $f = 1$ GHz. The OI configuration is shown in figure 1(a-b). For the first data set the medium is bounded within a PEC enclosure of radius of 0.12 m, while for second set the medium is unbounded. In both cases, the OI is illuminated by 32 transmitters at a frequency of $f = 1$ GHz and the data is collected using 32 receivers per transmitter. Transmitting and receiving antennas are evenly spaced on a circle of radius 0.1 m. The inversion domain $\mathcal{D}$ is a square centered in the middle of the enclosure with side lengths equal to 15 cm. For these results 3% noise was added to the synthetically generated scattered field data. The inversion mesh is unstructured consisting of arbitrarily oriented triangles and the number of nodes within $\mathcal{D}$ is 6027. The reconstructed permittivity after 1024 iterations is shown in figure 2(a-b) for the conductive enclosure case and in figure 2(c-d) for the unbounded problem. In both examples, the obtained contrast after each iteration is constrained to remain within physical bounds (*i.e.*, the real part of the relative permittivity is kept greater than one, and the conductivity is constrained to be a positive value). The execution time for each iteration was around 3 seconds on a PC workstation with two quad-core 2.8 GHz processors.

6. Conclusion

The FEM-CSI algorithm presented herein is an efficient inversion algorithm that allows one to (i) easily incorporate arbitrarily shaped conductive enclosures or simulate unbounded domain imaging setups, (ii) use an arbitrary irregular grid for the imaging region, and (iii) incorporate any inhomogeneous medium as a background reference. The resulting matrix equations are sparse and can be solved efficiently at each iteration. The use of arbitrarily shaped conductive enclosures to regularize the microwave tomography problem, and the use of an adaptive meshing scheme that refines the mesh at locations where more resolution is required, are topics of future research made possible by the use of FEM-CSI.

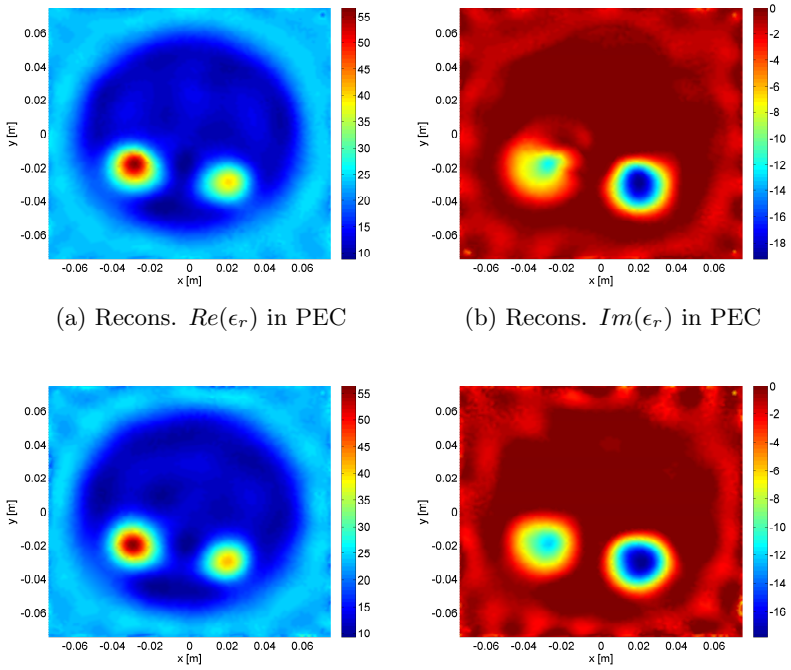

(a) Recons. $Re(\epsilon_r)$ in PEC (b) Recons. $Im(\epsilon_r)$ in PEC

(c) Recons. $Re(\epsilon_r)$ unbounded (d) Recons. $Im(\epsilon_r)$ unbounded

Fig. 2. Relative permittivity reconstructions of OI in PEC (a-b) and free-space (c-d).

7. Acknowledgment

The authors acknowledge the financial support of NSERC, MITACS, CancerCare Manitoba, and the University of Manitoba. We also thank Mr. Puyan Mojabi for fruitful discussions.

8. References

[1] P. M. van den Berg and R. E. Kleinman, "A contrast source inversion method," *Inverse Problems*, vol. 13, pp. 1607-1620, December 1997.

[2] C. Gilmore, A. Abubakar, W. Hu, T. M. Habashy, and P. M. van den Berg, "Microwave biomedical data inversion using the finite-difference contrast source inversion method," *IEEE Transactions on Antennas and Propagation*, vol. 57, no. 5, pp. 1528-1538, May 2009.

[3] A. Abubakar, W. Hu, P. M. van den Berg, and T. M. Habashy, "A finite-difference contrast source inversion method," *Inverse Problems*, vol. 24, December 2008.

[4] P. Mojabi, C. Gilmore, A. Zakaria, and J. LoVetri, "Biomedical microwave inversion in conducting cylinders of arbitrary shapes," *ANTEM/URSI 2009*, February 2009.

[5] J. Jin, *The finite element method in electromagnetics*, John Wile & Sons, Inc., New York, second edition, 2002.